

Analysis of hybrid mode-locking of two-section quantum dot lasers operating at 1.5 μm

Martijn J.R. Heck^{1,2,3,*}, Edcel J. Salumbides¹, Amandine Renault¹, Erwin A.J.M. Bente², Yok-Siang Oei², Meint K. Smit², René van Veldhoven², Richard Nötzel², Kjeld S.E. Eikema¹ and Wim Ubachs¹

¹Laser Centre Vrije Universiteit, 1081 HV Amsterdam, The Netherlands

²COBRA Research Institute, Technische Universiteit Eindhoven, Den Dolech 2, 5600 MB Eindhoven, The Netherlands

³Currently with the Department of Electrical and Computer Engineering, University of California Santa Barbara, Santa Barbara, CA 93106 USA

*mheck@ece.ucsb.edu

Abstract: For the first time a detailed study of hybrid mode-locking in two-section InAs/InP quantum dot Fabry-Pérot-type lasers is presented. The output pulses have a typical upchirp of approximately 8 ps/nm, leading to very elongated pulses. The mechanism leading to this typical pulse shape and the phase noise is investigated by detailed radio-frequency and optical spectral studies as well as time-domain studies. The pulse shaping mechanism in these lasers is found to be fundamentally different than the mechanism observed in conventional mode-locked laser diodes, based on quantum well gain or bulk material.

©2009 Optical Society of America

OCIS codes: (130.0250) Optoelectronics; (140.4050) Mode-locked lasers; (140.5960) Semiconductor lasers; (250.5590) Quantum-well, -wire and -dot devices

References and links

1. R. Kaiser, and B. Hüttl, "Monolithic 40-GHz mode-locked MQW DBR lasers for high-speed optical communication systems," *IEEE J. Sel. Top. Quant. Electron.* **13**, 125–135 (2007).
2. R. G. Broeke, J. Cao, C. Ji, S.-W. Seo, Y. Du, N. K. Fontaine, J.-H. Baek, J. Yan, F. M. Soares, F. Olsson, S. Lourduoss, A.-V. H. Pham, M. Shearn, A. Scherer, and S. J. B. Yoo, "Optical-CDMA in InP," *IEEE J. Sel. Top. Quant. Electron.* **13**, 1497–1507 (2007).
3. N. K. Fontaine, R. P. Scott, J. Cao, A. Karalar, W. Jiang, K. Okamoto, J. P. Heritage, B. H. Kolner, and S. J. B. Yoo, "32 Phase X 32 amplitude optical arbitrary waveform generation," *Opt. Lett.* **32**(7), 865–867 (2007).
4. B. Jalali, and S. Fathpour, "Silicon Photonics," *IEEE J. Lightwave Technol.* **24**(12), 4600–4615 (2006).
5. B. R. Koch, A. W. Fang, O. Cohen, and J. E. Bowers, "Mode-locked silicon evanescent lasers," *Opt. Express* **15**(18), 11225–11233 (2007).
6. H. Guo, K. Sato, K. Takashima, and H. Yokoyama, "Two-photon bio-imaging with a mode-locked semiconductor laser," in *Proceedings of 15th Internat. Conf. on Ultrafast Phenomena* (2006) paper TuE8.
7. K. W. Holman, D. J. Jones, J. Ye, and E. P. Ippen, "Orthogonal control of the frequency comb dynamics of a mode-locked laser diode," *Opt. Lett.* **28**(23), 2405–2407 (2003).
8. E. U. Rafailov, M. A. Cataluna, W. Sibbett, N. D. Il'inskaya, Y. M. Zadiranov, A. E. Zhukov, V. M. Ustinov, D. A. Livshits, A. R. Kovsh, and N. N. Ledentsov, "High-power picosecond and femtosecond pulse generation from a two-section mode-locked quantum-dot laser," *Appl. Phys. Lett.* **87**(8), 081107 (2005).
9. M. G. Thompson, D. Larson, A. R. Rae, K. Yvind, R. V. Penty, I. H. White, J. Hvam, A. R. Kovsh, S. S. Mikhlin, D. A. Livshits, and I. L. Krestnikov, "Monolithic hybrid and passive mode-locked 40 GHz quantum dot laser diodes," in *Proceedings of the European Conference on Optical Communication ECOC*, (Cannes, France, 2006) paper We4.6.3.
10. M. Kuntz, G. Fiol, M. Lammlin, D. Bimberg, M. G. Thompson, K. T. Tan, C. Marinelli, R. V. Penty, I. H. White, V. M. Ustinov, A. E. Zhukov, Y. M. Shernyakov, and A. R. Kovsh, "35 GHz mode-locking of 1.3 μm quantum dot lasers," *Appl. Phys. Lett.* **85**(5), 843 (2004).
11. E. U. Rafailov, M. A. Cataluna, and W. Sibbett, "Mode-locked quantum-dot lasers," *Nat. Photonics* **1**(7), 395–401 (2007).
12. D. Bimberg, M. Grundmann, F. Heinrichsdorff, N. N. Ledentsov, V. M. Ustinov, A. E. Zhukov, A. R. Kovsh, M. V. Maximov, Y. M. Shernyakov, B. V. Volovik, A. F. Tsatsul'nikov, P. S. Kop'ev, and Zh. I. Alferov, "Quantum dot lasers: breakthrough in optoelectronics," *Thin Solid Films* **367**(1-2), 235–249 (2000).
13. M. Kuntz, G. Fiol, M. Laemmlin, Ch. Meuer, and D. Bimberg, "High-speed mode-locked quantum-dot lasers and optical amplifiers," *Proc. IEEE* **95**(9), 1767–1778 (2007).
14. F. Lelarge, B. Dagens, J. Renaudier, R. Brenot, A. Accard, F. van Dijk, D. Make, O. le Gouezigou, J.-G. Provost, F. Poingt, J. Landreau, O. Drisse, E. Derouin, B. Rousseau, F. Pommereau, and G.-H. Duan, "Recent advances

- on InAs/InP quantum dash based semiconductor lasers and optical amplifiers operating at 1.55 μm ,” *IEEE J. Sel. Top. Quant. Electron.* **13**, 111–124 (2007).
15. C. Gosset, K. Merghem, A. Martinez, G. Moreau, G. Patriarache, G. Aubin, A. Ramdane, J. Landreau, and F. Lelarge, “Subpicosecond pulse generation at 134 GHz using a quantum-dash-based Fabry-Perot laser emitting at 1.56 μm ,” *Appl. Phys. Lett.* **88**(24), 241105 (2006).
 16. Z. G. Lu, J. R. Liu, S. Raymond, P. J. Poole, P. J. Barrios, and D. Poitras, “312-fs pulse generation from a passive C-band InAs/InP quantum dot mode-locked laser,” *Opt. Express* **16**(14), 10835–10840 (2008).
 17. J. P. Tournenc, A. Akrou, K. Merghem, A. Martinez, F. Lelarge, A. Shen, G. H. Duan, and A. Ramdane, “Experimental investigation of the timing jitter in self-pulsating quantum-dash lasers operating at 1.55 μm ,” *Opt. Express* **16**(22), 17706–17713 (2008).
 18. M. J. R. Heck, A. Renault, E. A. J. M. Bente, Y.-S. Oei, M. K. Smit, K. S. E. Eikema, W. Ubachs, S. Anantathanasarn, and R. Nötzel, “Passively mode-locked 4.6 GHz and 10.5 GHz quantum dot laser diodes around 1.55 μm with large operating regime,” *IEEE J. Sel. Top. Quant. Electron.* **15**, 634–643 (2009).
 19. M. J. R. Heck, E. A. J. M. Bente, B. Smalbrugge, Y.-S. Oei, M. K. Smit, S. Anantathanasarn, and R. Nötzel, “Observation of Q-switching and mode-locking in two-section InAs/InP (100) quantum dot lasers around 1.55 μm ,” *Opt. Express* **15**(25), 16292–16301 (2007).
 20. A. Shen, F. van Dijk, J. Renaudier, G. H. Duan, F. Lelarge, F. Pommereau, F. Poingt, L. Le Gouezigou, and O. Le Gouezigou, “Active mode-locking of quantum dot Fabry-Perot laser diode,” in *Proceedings IEEE 20th International Semiconductor Laser Conference* (2006) pp. 153–154, paper ThB6.
 21. G. Girault, M. Gay, S. Lobo, L. Bramerie, M. Joindot, J. C. Simon, A. Shen, F. Blache, H. Gariah, F. Mallécot, O. Le Gouezigou, F. Poingt, L. Le Gouezigou, F. Pommereau, B. Rousseau, F. Lelarge, and G.-H. Duan, “Quantum dash actively modelocked Fabry-Perot laser module demonstrated as part of wavelength tunable RZ transmitter,” *Electron. Lett.* **44**(14), 873–874 (2008).
 22. K. A. Williams, M. G. Thompson, and I. H. White, “Long-wavelength monolithic mode-locked diode lasers,” *N. J. Phys.* **6**, 179 (2004).
 23. S. Anantathanasarn, R. Nötzel, P. J. van Veldhoven, F. W. M. van Otten, Y. Barbarin, G. Servanton, T. de Vries, E. Smalbrugge, E. J. Geluk, T. J. Eijkemans, E. A. J. M. Bente, Y. S. Oei, M. K. Smit, and J. H. Wolter, “Lasing of wavelength-tunable (1.55- μm region) InAs/InGaAsP/InP (100) quantum dots grown by metal organic vapor-phase epitaxy,” *Appl. Phys. Lett.* **89**(7), 073115 (2006).
 24. D. von der Linde, “Characterization of the noise in continuously operating mode-locked lasers,” *Appl. Phys. B* **39**(4), 201–217 (1986).
 25. F. R. Ahmad, and F. Rana, “Fundamental and subharmonic hybrid mode-locking of a high-power (220 mW) monolithic semiconductor laser,” *IEEE Photon. Technol. Lett.* **20**(15), 1308–1310 (2008).
 26. L. A. Jiang, “Ultralow-noise modelocked lasers,” (Ph.D. diss., Massachusetts Institute of Technology, 2002).
 27. A. J. Lowery, N. Onodera, and R. S. Tucker, “Stability and spectral behavior of grating-controlled actively mode-locked lasers,” *IEEE J. Quantum Electron.* **27**(11), 2422–2430 (1991).
 28. K. Yvind, “Semiconductor mode-locked lasers for optical communication systems,” (Ph.D. diss., Technical University of Denmark, 2003).
 29. A. Akrou, A. Shen, R. Brenot, F. Van Dijk, O. Lelouezigou, F. Pommerau, F. Lelarge, A. Ramdane, and G.-H. Duan, “Error-free transmission of 8 WDM channels at 10 Gbit/s using comb generation in a quantum dash based mode-locked laser,” in *Proceedings 34th European Conference on Optical Communication ECOC* (Brussels, Belgium, 2008) paper Th3D4.

1. Introduction

Mode-locking of laser diodes is a well-established technique for generating short optical pulses at wavelengths around 1.55 μm . These wavelengths are of primary interest for telecommunication applications. Mode-locked laser diodes (MLLDs) can be used as high-speed sources in e.g. optical time-domain multiplexed and wavelength-division multiplexed systems [1]. Current interest in these MLLDs lies in utilizing the coherent bandwidth that these lasers generate in combination with mature optical fiber-based technology in advanced optical (telecommunication) systems, such as optical code-division multiple-access systems [2], arbitrary waveform generation [3], clock distribution and as multi-wavelength sources for silicon-based integrated optics [4,5]. Moreover these MLLDs have found their way to other fields of research, such as biophotonics, since these wavelengths can have a larger penetration depth into human tissue [6], and frequency comb generation [7], e.g. for metrology purposes.

Many of these applications require the coherent optical bandwidth of the MLLD to be broad and the output pulse train to be stable in time, with a minimum of phase and amplitude fluctuations. Quantum dot (QD) material has been shown to be promising as a gain medium for (monolithic) MLLDs as compared to bulk or quantum well gain material. The inhomogeneous broadening leads to a broad gain spectrum, which can in principle lead to ultra-short pulse generation [8]. The QDs show reduced amplified spontaneous emission as compared to bulk or quantum wells. This leads to reduced phase and amplitude noise and

consequently to a reduced timing jitter [9,10]. An overview of mode-locked quantum dot lasers can be found in [11].

Many of these advantages have been reported with two-section MLLDs containing an optical amplifier and saturable absorber section, that are based on In(Ga)As/GaAs QD gain material. These lasers operate in the 1.2- μm to 1.3- μm wavelength region [12,13]. Results obtained with InAs/InP QD material in the 1.5- μm region are scarcer. State-of-the-art results at these wavelengths have been obtained with quantum dash gain material [14]. Although strictly speaking these quantum dashes, or elongated dots, are not true zero-dimensional structures, they share a lot of beneficial and typical characteristics with QDs, such as spatial carrier confinement. Passive mode-locking has been achieved in single section InAs/InP QD and dash devices. Subpicosecond pulse generation [15,16] and low timing jitter [17] have been observed. We have shown previously that the regime of stable mode-locking in two-section MLLDs can be an order of magnitude larger than those of multi-quantum well or bulk gain material based MLLDs. This is essential for practical implementation of such devices as this makes them more tolerant against variations in operating parameters [18]. However the output pulses we have observed from our devices are very elongated [18,19] up to the point that the instantaneous output power varies by only a fraction of the total output power. Thus pulse lengths are close to the roundtrip length of the cavity while the pulses are also highly chirped, with chirp values of up to 20 ps/nm. This mode of operation may be looked upon as being close to what is sometimes called Fourier domain or FM mode-locking. The operation of our devices has significant similarities with the operation of single section quantum dash lasers reported in [17]. Pulses can only be observed after filtering the output [17,18] or compression by a dispersive element [19].

There have only been a few efforts on active and hybrid mode-locking of these InAs/InP QD MLLDs, e.g [20,21]. From an application point of view the synchronization with an external clock is often essential, e.g. for clock distribution where repetition rate fine-tuning and timing jitter minimization are required. From a scientific point of view it is interesting how active mode-locking and especially hybrid mode-locking in a two-section MLLD influences the pulse shaping mechanism. For bulk and quantum well based MLLDs this mechanism is well understood, e.g [22]. Since the passive mode-locking mechanism driving the InAs/InP QD laser to its highly chirped state is not understood, the hybrid mode-locking might give us a better insight into the mechanism. We expect a far stronger impact of hybrid mode-locking in the case of these QD MLLDs in comparison to the case of quantum well lasers. In QD MLLs the output pulses are very elongated spanning a significant part of the laser cavity [19]. The synchronization with an electrical clock allows for a broader range of measurement techniques and, for example, a high bandwidth optical sampling oscilloscope can be used for characterization and analysis.

In this work for the first time an investigation of hybrid mode-locking in two-section InAs/InP QD Fabry-Pérot (FP) type MLLDs is presented. Hybrid mode-locking is defined as adding an electrical modulation, with a frequency close to the cavity free-spectral range, to a reversely biased intra-cavity saturable absorber (SA) section. This is unlike active mode-locking, where (part of) the gain section of the laser is modulated [20,21]. We will show that, hybrid mode-locking strongly decreases the pulse timing jitter from the values we obtained from passive mode-locking of these devices. This is not completely obvious given the unusual passively mode-locked operation. Moreover we will show that due to the inhomogeneous broadening and discrete energy level structure of the QD material these MLLDs behave strikingly different from their bulk, quantum-well or quantum-dash counterparts. We will show that the laser in its hybridly mode-locked state still shows an albeit shortened, highly chirped output pulse. This indicates the strength of the underlying mode-locking mechanism. An explanation is presented. In this paper first the device design and fabrication are presented in section 2. Hereafter the experimental results are presented and discussed (section 3), with an emphasis on the phase noise and its origin. The conclusions are then summarized in section 4.

2. Device and measurement setup

The QD laser structure is grown on n-type (100) InP-substrates by metal-organic vapor-phase epitaxy, as presented in [23]. Two-section FP-type MLLDs have been designed and fabricated in the same way as presented in [19]. These are ridge-waveguide lasers fabricated using reactive ion etching with a ridge width of 2 μm . The mirrors are formed by cleaved facets that are both uncoated. In this work we focus our attention on a device consisting of a 9-mm long cavity corresponding to a 4.5-GHz roundtrip frequency and having an SA-section of 270 μm . These devices are comparable to the lasers we have presented in [18,19]. The MLLD is then mounted on a ceramic submount with gold-plated transmission lines. The p-side of the SA is then wire-bonded to the signal line. This submount is mounted on a temperature controlled copper chuck. The SA is reversely biased through a ground-signal-ground probe and the gain section is forward biased through a needle probe.

The characterization setup used is depicted in Fig. 1. An anti-reflection coated lensed fiber is used to collect the laser output at the amplifier end of the laser and an optical isolator is used to prevent feedback from reflections into the laser cavity. A commercial semiconductor optical amplifier (SOA) is used to optionally boost the optical output power. An SOA is used because the operating wavelengths of the laser are around 1500 nm, i.e. outside of the range of the Erbium-doped fiber amplifier (EDFA)-window. The SOA is operated at a gain level of 6 dB – 7 dB.

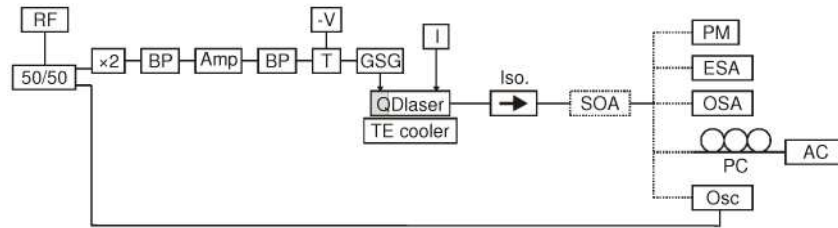


Fig. 1. Overview of the used setup. RF: Agilent N5181A generator; 50/50: signal splitter; x2: frequency doubler; BP: 3.0 – 4.3 GHz bandpass filter; Amp: electrical RF-amplifier; T: bias tee, -V: DC voltage source; GSG: ground-signal-ground probe; I: DC current source; Iso: optical isolator; SOA: semiconductor optical (booster) amplifier; PM: optical power meter; ESA: 26-GHz electrical spectrum analyzer with 12.5-GHz fast photodiode; OSA: 0.05-nm bandwidth optical spectrum analyzer; Osc.: Digital communications analyzer (digital sampling oscilloscope) with a 30-GHz optical module; PC: polarization controller; AC: autocorrelator. All equipment is fiber pigtailed or has fiber input or output connectors, except for the (free-space) fast photodiode.

3. Experimental results

The MLLD with a 270- μm SA is first characterized in the passively mode-locked regime, i.e. without an electrical RF-signal applied to the SA. Hereafter hybrid mode-locking is explored in the most promising regimes. The laser has a threshold injection current of 240 mA up to 255 mA for SA bias voltages of 0 V down to -2 V. The optical output power increases towards 10 mW at 800 mA SOA injection current. The optical spectra show that the output wavelengths are centered around 1.50 μm . The minimum RF-linewidths under passive modelocking are found around 380 mA injection current and -5 V SA bias voltage. This minimum width at -20 dB is between 4 MHz - 7 MHz. Increasing the injection current further broadens the RF-linewidths and destabilizes the mode-locking mechanism. This is due to the start of lasing on excited state (ES) transitions, as can be observed in the optical spectrum and much like described in [18].

3.1 Hybrid mode-locking

In Fig. 2 the electrical spectrum is shown for the MLLD with a 270- μm SA under hybrid mode-locking. The operating injection current and RF driving frequency have been optimized for maximum pedestal suppression (Fig. 2(b)), using an RF-power of 18 dBm (about 2.5 V

with 50- Ω load resistance). The synchronization with the RF-generator (Fig. 1) under hybrid mode-locking strongly decreases the low-frequency phase noise. This is indicated by the decrease in linewidth of the first harmonic peak in the RF spectrum from about 4 MHz – 7 MHz at –20 dB from the peak under passive mode-locking to the ~Hz-range, as limited by the RF-generator and analyzer (see Fig. 2(b)). To quantify the linewidth and shape that has been achieved, the single side-band (SSB) phase noise is given in Fig. 3, where it is compared to the phase noise of the generator. While up to 300 kHz offset the MLLD follows the phase noise of the generator, above 200 MHz offset the noise floor of the spectrum analyzer is dominant. Between 500 kHz and 30 MHz a clear plateau or pedestal can be observed. This plateau is at a level of –117 – –118 dBc/Hz for these operating conditions (Fig. 3). For comparison we investigated the level of the plateau at a lower SA voltage of –0.5 V (320 mA injection current) and found the level of this plateau to be one order of magnitude higher, i.e. around –106 dBc/Hz. All further results reported are with an SA bias of –4.6 V and an injection current of 386 mA, unless otherwise noted, since these operation conditions show the lowest phase noise, as expressed e.g. by the level of the aforementioned plateau. This is further quantified below.

From the phase noise spectrum the timing jitter is calculated using the method presented in [24]. The contribution of the amplitude modulation in the RF spectrum is ignored, since the plateau in the phase noise plot around the DC-peak is below the noise floor of the RF analyser and hence significantly lower than the pedestal for the first harmonic. Therefore to obtain an upper limit estimation to the timing jitter the SSB phase noise around the first harmonic can be integrated. The calculated value for the timing jitter is less than 0.6 ps for the 10 kHz – 300 MHz integration range and about 0.5 ps for the 10 MHz – 300 MHz integration range, indicating that the major contribution to the phase noise is in this latter range. A more detailed evaluation of the phase noise, including an evaluation of the higher harmonics, is given below.

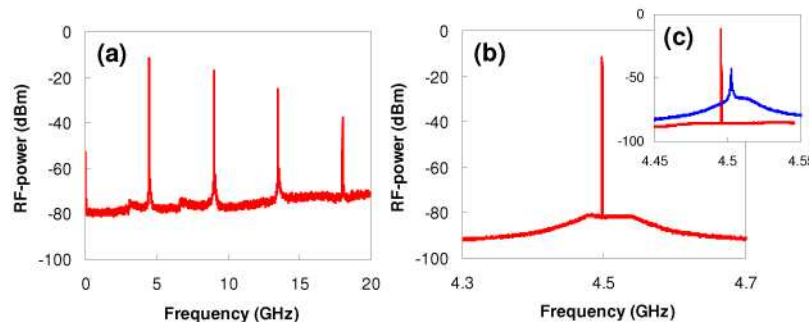


Fig. 2. (a) RF-spectrum obtained for the 4.5-GHz laser with 270- μ m SA length. Injection current is 386 mA and SA bias voltage is –4.6 V. (b) Detailed view of the spectrum around the first RF-peak in (a). Inset (c) shows the comparison with the passively mode-locked RF peak (blue). The electrical bandwidths used to obtain the spectra are 3 MHz, 100 kHz and 50 kHz for (a), (b) and (c) respectively. RF-power is 18 dBm and RF driving frequency is 4.496 GHz.

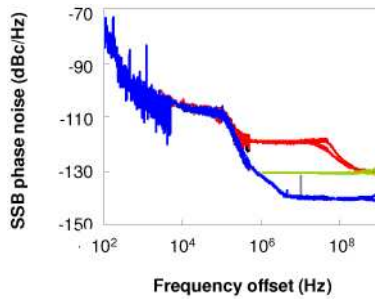


Fig. 3. Single side-band phase noise plot (left and right sideband overlaid) around the first harmonic at 4.5 GHz in Fig. 2 (red). The generator noise (blue) and the analyzer noise floor (green) are also shown. Operating conditions are as in Fig. 2. In the analysis of the generator noise, the power of the first harmonic was maximized for optimum signal-to-noise ratio, hence the lower noise floor.

In previous studies on hybrid mode-locking the level of the phase noise plateau (appearing between 500 kHz and 30 MHz in Fig. 3) was found to decrease with increasing modulation depths of the SA [25,26]. In this frequency range it actually scales inversely proportional to the square of the optical loss modulation depth M . In Fig. 4(a) the level of the plateau is shown as a function of the RF-driving power. These values for the plateau suppression are comparable to the values reported for MLLDs with similar repetition rates, e.g [25]. The linear fit through the (double-log scale) data set has a slope of -1.4 . Since theory [26] predicts a slope of -2 for the dependency of the phase noise pedestal on the modulation depth, we conclude that the optical loss modulation depth scales as $M \propto P_{RF}^{0.7} \propto V_{SA}^{1.4}$, with P_{RF} the RF-driving power. Note that for electro-absorption modulation the relation $M \propto V$ is generally not valid, unlike e.g. electro-optic modulation [26].

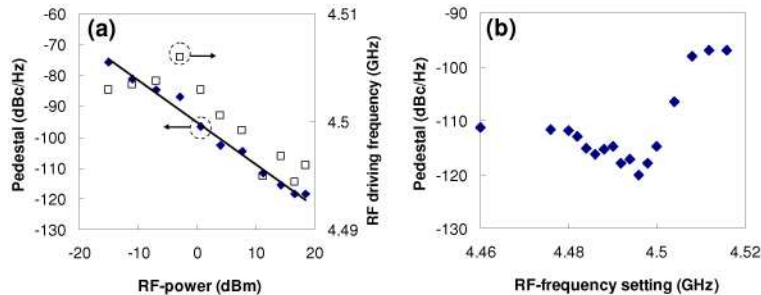


Fig. 4. (a) Optimized plateau suppression (diamonds) as a function of the RF driving power at the frequencies indicated (squares) and (b) as a function of the RF driving frequency at a power of 18 dBm. Further operating conditions are as in Fig. 2.

3.2 Locking range of hybrid mode-locking

For practical applications it is convenient but also necessary to be able to fine-tune the pulse repetition rate. In Fig. 4(b) the plateau suppression as a function of the RF driving frequency is shown. We define the locking range as the frequency range in which the pedestal suppression is within 3 dB of its optimal value. This 3-dB locking range for this laser is 8 MHz, which is at least two orders of magnitude better than the results obtained with a single-section actively QD mode-locked laser at $1.5 \mu\text{m}$ [20]. This suggests there is a clear advantage for a two-section MLLD, where under hybrid mode-locking the modulation is localized within a small part of the cavity, i.e. the SA section, as opposed to active mode-locking of a single-section monolithic device [20,21]. In quantum well MLLDs the explanation for the limited locking range is that the gain window has a maximum before (after) the pulse when the driving frequency is too high (low). This results in the build-up of parasitic pulses before (after) the main pulse, which grow at the expense of the old pulse [27]. We will further

investigate the link between the position of the RF driving frequency within the locking range, the RF power and the optical spectrum.

Looking at the optical spectra we can see that there is a significant change when the driving power is changed. In Fig. 5(a) it can be seen that the spectrum is extended by 3 nm towards the long-wavelength side when the driving power is increased from 4 dBm to 18 dBm. There is only a small change (0.5 nm – 0.8 nm) on the short-wavelength side of the spectrum. Note that in Fig. 5(a) the driving frequency is kept constant at the value for optimum locking at 18 dBm.

When the driving frequency is changed, a similar effect on the optical spectra is observed. In Fig. 5(b) it can be seen that the long wavelength side of the spectrum is shifting by about 3 nm to longer wavelengths, when the driving frequency is increased over 56 MHz from 4.460 GHz to 4.516 GHz. For the optimal locking range, with the lowest phase noise plateau (4.490 GHz – 4.500 GHz, see Fig. 4(b)) this shift is 1.9 nm. The change on the short-wavelength side is about 1.7 nm – 1.9 nm over the 4.460 GHz to 4.516 GHz locking range, in the same direction, meaning that the spectrum shifts to the longer wavelengths. We attribute this effect at least partially to the group velocity dispersion of the QD gain material. In similar QD laser structures [18,19] that are operated close to threshold, we have measured the group index of the QD amplifier waveguide to vary with wavelength according to (Cauchy expression): $n_g = n_0 + n_1/\lambda^2$, with $n_0 \approx 2.4$ and $n_1 \approx 3.0 \cdot 10^{-12} \text{ m}^2$. This means that the group index changes by about 0.05% per nanometer close to $\lambda = 1.5 \text{ }\mu\text{m}$. Over the optimum locking range (4.49 GHz up to 4.50 GHz) the spectral shift is 1.9 nm towards the longer wavelengths. The corresponding group index decreases by about 0.1% over this 1.9-nm shift, i.e. the pulse will speed up by 0.1%. This value can be compared to the 0.2% change in driving frequency, i.e. over 10 MHz from 4.49 GHz to 4.50 GHz. The finite gain bandwidth and SA absorption bandwidth prevent a full shift of the spectrum.

The red-shift of the spectrum with increasing RF driving power cannot directly be explained by the group-velocity-dispersion as described above, since the driving frequency is kept constant (Fig. 5(a)). In hybrid mode-locking the SA section will be driven in a lower absorption state and the absorption in the cavity is effectively lowered. This explains the observation of a 0.5-dB increase in the output power when the MLLD is operated under hybrid mode-locking instead of passive mode-locking. We hypothesize that the reason for the red shift at higher RF powers is the fact that the leading edge red wavelengths (Fig. 6 and [18,19]) are absorbed during passive mode-locking in the process of saturating the SA, whereas in hybrid mode-locking this absorption is decreased due to the lower voltage over the SA (during the ‘open’ part of the cycle of the RF-driving signal). The shift towards shorter wavelengths of the right-hand-side of the spectrum with decreasing RF-driving power can then be explained by the fact that the system behaves increasingly like a passively mode-locked system.

3.3 Chirp evaluation

In our previous work [18,19] we have observed the unique operation of the passive mode-locking of these 1.5 μm QD lasers which led to extremely large upchirp over the generated pulses. These observations show many similarities with the results obtained with quantum dash MLLDs [17]. To obtain the chirp profile of the pulses produced with hybrid mode-locking we use a similar approach as in [18,19]. The setup is shown in Fig. 6(a). A 30 GHz bandwidth photodiode-sampling oscilloscope combination is triggered by the RF-generator and the spectrally filtered pulse is monitored. When the 1.2-nm bandpass filter is tuned, the position of the pulse on the oscilloscope will change as a result of the chirp of the pulse. The results for the delay are shown in Fig. 6(b). It can be seen that the pulse has an upchirp, with a value of about 8 ps/nm using a linear approximation of the chirp profile. However there are higher order contributions to the chirp.

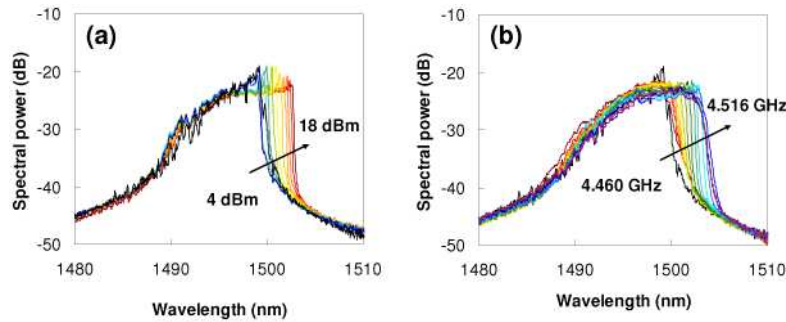


Fig. 5. (a) Optical spectra as a function of the RF driving power at a frequency of 4.496 GHz and (b) as a function of the RF driving frequency at a power of 18 dBm, corresponding to the datapoints in Fig. 4. For reference the spectra under passive mode-locking are given (black).

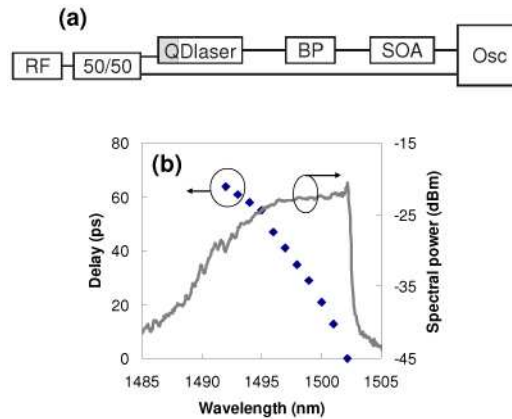


Fig. 6. (a) Setup to measure the delay of the different spectral components. The 4-GHz oscilloscope is triggered on the signal from the RF-generator and the pulse position is monitored as a function of its wavelength, as determined by the 1.2-nm optical bandpass filter (BP) (b) Measured delay (blue diamonds) of the filtered signal as compared to the filtered signal at 1503 nm. The optical spectrum is shown for reference (grey solid line).

To verify this chirp profile we compress the pulse using single mode fibre and use an autocorrelator to measure the pulse shape. Directly at the laser output (using only a few meters of optical fiber) the duration of the second-harmonic generated (SHG) signal is about 66 ps. Adding pieces of standard single-mode optical fiber (SMF) with a dispersion of 14 – 16 ps/nm·km at 1.5 μm to the output of the laser should then compress the pulses. This is indeed the case, as can be seen in Fig. 7, and a minimum of about 2-ps pulse duration (deconvolved) can be found starting around 500 m SMF and extending to 700 m SMF. This is in close agreement with the expected value of (535 ± 35) m based on the 8 ps/nm chirp observation. We note that higher order chirp components prevent full compression of the pulses into the sub-picosecond regime, i.e. close to transform limited, when only the dispersion of SMF is used, which is mainly of second order. Higher order dispersion is also the reason for the broad minimum in Fig. 7(b). The pulse shaping and compression is verified with a 30-GHz digital communication analyzer in Fig. 7(c), where clearly compression down to the bandwidth limit of the analyzer can be observed. Furthermore the timing jitter measured by this analyzer was 1.2 ps, which was the limit of the analyzer.

The most interesting fact is that the laser keeps on operating under hybridly modelocking in this remarkable highly chirped way over a similar bandwidth value. The output pulse length is shortened from a near CW total output in the passive mode-locked situation by the hybrid mode-locking to approximately a third of the roundtrip time. This shows that the mechanism that is driving the chirp is a strong mechanism.

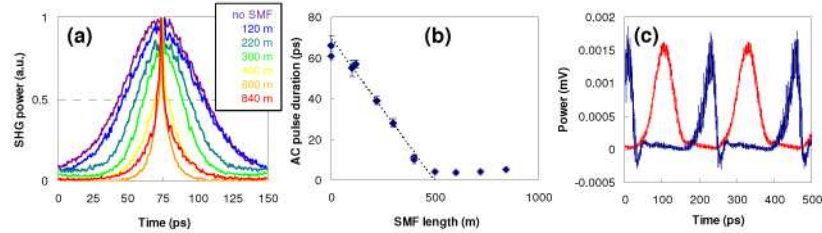


Fig. 7. (a) Autocorrelator traces obtained with different lengths of SMF at the MLLD output, ranging from 0 m to 840 m, as indicated in the legend. The traces have been normalized. The duration of the SHG signals as a function of the SMF lengths is plotted in (b). (c) 30-GHz digital sampling oscilloscope trace of the pulse without compression (red) and with 840 m of SMF (blue).

3.4 Phase noise evaluation

The phase noise of MLLDs is commonly quantified by studying the single-side-band phase noise of the first harmonic [17,26,28]. In this way an upper limit of the timing jitter can be determined. A more thorough treatment of the noise includes a study of the higher harmonics. By comparing the noise pedestals of the harmonics, amplitude and timing noise can be separated, using the method developed by Von der Linde [24]. This technique is however based on a number of assumptions, e.g. that the pulse shape is constant.

In Fig. 8 the first four harmonics of the RF-spectrum of the MLLD under hybrid mode-locking have been plotted, using the same operation conditions as mentioned above. Three main points can be made. First the increase of the noise pedestal does not scale quadratically with the harmonic number, as is predicted by the Von-der-Linde model. Secondly the pedestals show a structure with added noise bumps, unlike what might be expected from purely broadband ASE noise-induced fluctuations in the output. The conclusion is that richer dynamics take place, a phenomenon that we also observed with the passive mode-locking of these MLLDs [18]. Thirdly the DC-pedestal (Fig. 2) which is caused by amplitude noise only, is about 8 dB lower than the pedestal around the first harmonic. An integration over the SSB phase noise then represents the timing jitter without a significant contribution from the amplitude modulation [24].

To further investigate these dynamics, measurements are performed at limited optical bandwidths for which a variable optical bandpass filter of 1.2 nm width is employed. In Fig. 9 the resulting RF-spectra are shown when the position of the filter is varied. The first obvious point that can be made is that the noise pedestals are dramatically increased as compared to Fig. 8, i.e. by about 20 dB for the leading edge wavelengths (around 1500 nm) up to over 40 dB for the trailing wavelengths (close to 1490 nm). Since these pedestals are also present around the DC-component, this means that the filtered output experiences a large amplitude modulation. As noted above the unfiltered, full-bandwidth output of the MLLD shows no visible trace of amplitude modulation around the DC-peak above the noise floor of the spectrum analyzer. The observed pedestals are significantly lower (by 20 dB – 40 dB) for the full-bandwidth output of the MLLD as compared to the filtered output. To account for this difference we conclude that power exchange takes place between the different spectral components of the MLLD output and the total pulse energy is nearly constant. This phenomenon is also observed in e.g. quantum dash lasers [29], where it is ascribed to mode partition noise.

Looking more closely at the shape of the pedestals in the filtered signal, we can discern three different regimes. The leading edge, i.e. longer wavelength, optical spectral components (1503 nm) have a pedestal in the RF spectrum around the fundamental peak that decreases in height with offset frequency, as can be expected from noise induced broadening (in this case with approximately $1/f$ dependency, unlike the typical $1/f^2$ dependency observed in MLLDs [25]). The optical spectral components in the range 1501 nm – 1497 nm, show clear sidebands around the fundamental RF-peaks at 170 MHz down to 100 MHz respectively. The trailing

spectral components 1495 nm – 1491 nm again show the noise decreasing with offset frequency and the sidebands have merged into a single pedestal. We note that the RF-peak is slightly off the center of the noise pedestal, to the lower frequency side. This can be expected since the free-running laser, without RF-driving signal has a natural frequency which is slightly higher, as was mentioned above.

This evaluation of the noise pedestals in the filtered signal is very useful to gain insight into the pulse shaping mechanism in the MLLD. Noise sidebands, as seen in the 1501 nm – 1497 nm region, are an indication of cyclic amplitude and/or timing instabilities. In hybrid mode-locking of bulk or quantum-well MLLDs these instabilities are well-known to occur when the RF-driving frequency runs out of the locking range. As a result parasitic pulses at the trailing or leading edge of the main pulse can build up, gaining power and take over from the main pulse, as observed and explained in [27]. We explain our observations by making use of this characteristic behavior.

Due to the group velocity dispersion, the longer-wavelength spectral components of the pulse propagate at a higher group velocity than the shorter-wavelength spectral components. From Fig. 6 it is inferred that the longer wavelengths lead the shorter wavelengths. We hypothesize that the pulse shaping starts at the longer wavelengths, i.e. around 1503 nm, and the RF-driving frequency is synchronized to their roundtrip frequency. In their trail these wavelengths ‘open’ a gain window, since they saturate the SA. Consequently, the trailing wavelengths can build up to a pulse. So the leading edge, longer-wavelength spectral component of the pulse is followed by a train of increasingly shorter-wavelength spectral components of the pulse. Coherence between these spectral components is maintained because of the homogeneous broadening. However since the trailing spectral components have a lower group velocity than the leading ones, the total (full-bandwidth) pulse is pulled apart. As a result the trailing spectral components run out of the gain window that was created by their leading ones and consequently instabilities, such as the build-up of parasitic pulses (spectral components), arise, much like reported in [27]. Since this is a cyclic dynamic behavior this explains the appearance of the sidebands at 100 MHz – 170 MHz.

On the trailing edge of the pulse, i.e. at wavelengths 1495 nm – 1491 nm, the sidebands have disappeared. We assume that the modulations are suppressed by the RF-driving voltage. This (sinusoidal) driving voltage increases at the trailing end of the pulse, effectively closing the gain window. The wavelengths at the trailing end of the pulse will be absorbed more easily if they fall behind too much. It is energetically more favorable to keep the trailing part of the pulse together to bleach the SA and the energy of the trailing components is effectively pushed forward by this mechanism to keep up with the leading edge. This result can be related to Fig. 6(b), which shows that the chirp decreases near the trailing edge of the pulse.

In conclusion it can be said that the instabilities in the pulse shaping mechanism in these kinds of lasers are dominated by power exchange between different spectral components within the full bandwidth of the laser. We have given a qualitative explanation for this phenomenon. Since the spectral components are spatially (or temporally) separated from each other due to the high chirp of the output pulse, this power exchange between spectral components translates to a power exchange between different spatial components of the pulse. As a result the energy distribution within the pulse and consequently the center of gravity of the energy of the pulse can fluctuate. This would then increase the phase noise of the full-bandwidth output. The question is then what will happen when the spatial separation of the spectral components is minimized, i.e. in the case where the pulse is compressed (Fig. 7). This is explored in the next paragraph.

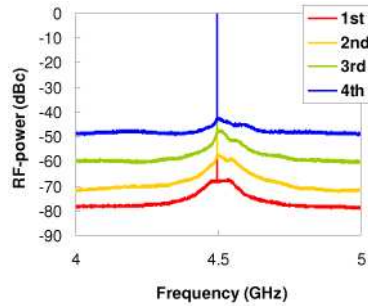


Fig. 8. Close up of the first four harmonics from Fig. 2(a), normalized to the respective carrier peak. Spectra have been obtained with a 200-kHz resolution. The same operating conditions were used as in Fig. 2. The higher harmonics have been shifted in frequency and have been centered around the first harmonic.

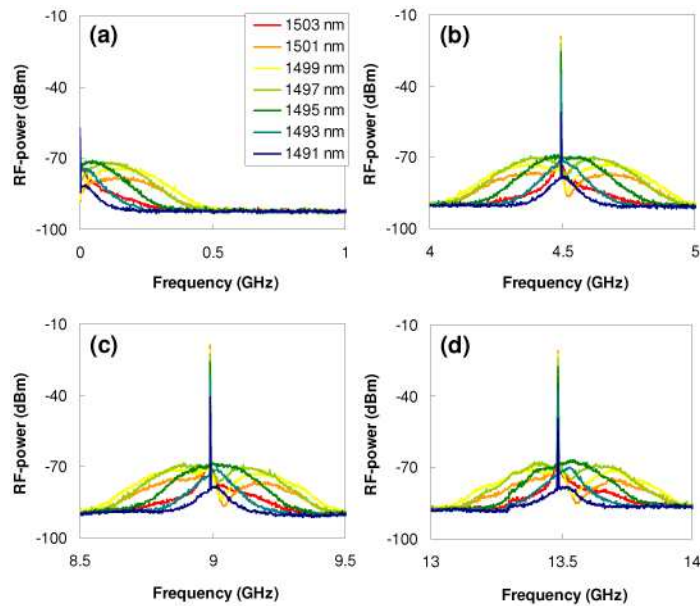


Fig. 9. RF-spectra obtained after filtering the output with a 1.2-nm optical bandpass filter centered at the spectral positions as indicated in the legend and representing (a) the DC-peak and (b – d) the first three harmonics respectively. The resolution used was 100 kHz. The same operating conditions were used as in Fig. 3.

3.5 Evaluation of the power exchange

Again the pulse is compressed by using different lengths of SMF, as mentioned in Fig. 7. Figure 10 shows the electrical spectra around the first harmonic of the output after propagation through different lengths of SMF. Three important points can be made. First of all, with no added dispersion, the pulse pedestal is asymmetric around the RF driving frequency and has a maximum at around 20 MHz to the higher frequency side of the peak. This means that within a pulse, energy is being transferred from the trailing edge to the leading edge in a 20-MHz cyclic way. Or, vice versa, a dip in the energy is being transferred from the leading edge to the trailing edge of the pulse. So it is clear that power exchange between different temporal or spatial components of the pulse takes place.

Since the pulse is heavily chirped, the temporal components translate to spectral components. As a second point it can be noted that at a dispersion of 2 ps/nm, i.e. 100 m SMF, the pedestal around the main RF driving peak becomes symmetric and the maximum at

20 MHz higher frequency is suppressed. So it is clear that the energy exchange between the spectral components causes the energy exchange between temporal components of the pulse.

As a third point it can be noted that at higher dispersion values (using between 200 m and 840 m SMF, see Fig. 10), the pedestal becomes asymmetric again, but now a maximum appears to the lower frequency side, around 10 – 20 MHz from the driving RF peak. This means that the energy transfer within the pulse goes the opposite way around as compared to the case without dispersion at the output. A full analysis of these dynamics would require high-speed real-time characterization of the temporal profile of the different spectral components, e.g. as presented in [18], which is beyond the scope of this paper.

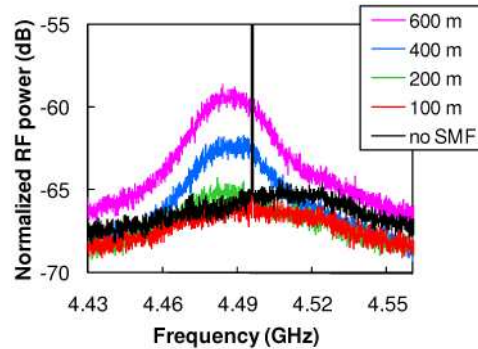


Fig. 10. RF spectra normalized with respect to the carrier peak. The spectra have been obtained for the optical output after a length of SMF, as indicated in the plot. The electrical bandwidth used was 50 kHz. Operation conditions are $V_{SA} = -4.9$ V, $I = 380$ mA. RF-power is 18 dBm and RF driving frequency is 4.496 GHz.

4. Conclusion

In this work we have for the first time presented a detailed study of hybrid mode-locking in two-section InAs/InP QD FP-type MLLDs. First and foremost the hybrid mode-locking is able to stabilize the pulse timing jitter to around 0.6 ps (10 kHz – 300 MHz range). Although this value is comparable to state of the art for monolithic, 5-GHz lasers [25], lower values can be expected due to the low ASE generation in these QD MLLDs. The output pulses are heavily upchirped, with a value of 8 ps/nm, using a linear approximation of the chirp profile. The optical output bandwidth is relatively large at 8 nm FWHM. Pulse compression down to 2 ps is feasible using the second order dispersion of SMF. The MLLDs have to be operated close to threshold since increasing the current to much larger values increases the optical bandwidth too much for the lasers to operate in a stable mode.

The mechanism leading to the phase noise is investigated and it is concluded that power exchange between different spectral components of the pulse is at least partially responsible for the phase noise of the full-bandwidth of the pulse. This power exchange arises from slightly different propagation speeds of the different spectral components, leading to a cyclic dynamic behavior of the spectral components trailing the leading edge of the pulse. This leads us to conclude that the pulse shaping mechanism in these QD MLLDs is fundamentally different than the mechanism observed in conventional MLLDs based on quantum well or bulk gain material. Also InAs/GaAs QD MLLDs operating around $1.0 \mu\text{m} - 1.3 \mu\text{m}$ do not show such behavior [11]. We ascribe these effects to the relatively large inhomogeneous broadening and small homogeneous broadening of the InAs/InP QD gain medium.

Based on our analysis of the origin of phase noise we anticipate that the phase noise of these lasers can severely be suppressed when the cavity dispersion is minimized. Moreover we think that under such conditions stable operation with larger optical bandwidths, i.e. under larger injection currents, can be achieved. Suppression of the phase noise, and more specifically of the mode partition noise, is essential for applications where the MLLD is used as a multi-wavelength source [29] or arbitrary waveform generator [3], since this noise translates directly to noise on the signal. For applications like biomedical imaging by non-

linear microscopy [6] stable pulse-to-pulse peak power and pulse energy are required and the phase noise of the total output should be considered. The low amplitude noise makes this type of MLLD very useful for such an application, where a constant pulse energy is required. The effect of the mode partition noise on the fluctuations in peak power of the pulses after pulse compression is also an important issue for applications in nonlinear microscopy, but the study of this fluctuation is beyond the scope of this paper.

Acknowledgements

This work was supported by the Dutch Ministry of Economic Affairs under the National Research Combination (NRC) Photonics Grant and by the Smart Mix Program of the Netherlands Ministry of Economic Affairs and the Netherlands Ministry of Education, Culture and Science.